K_{ATP} Channel blockade instructs microglia to foster brain repair and neurogenesis after stroke

Fco. Javier Ortega González

K_{ATP} CHANNEL BLOCKADE INSTRUCTS MICROGLIA TO FOSTER BRAIN REPAIR AND NEUROGENESIS AFTER STROKE

Fco. Javier Ortega González

PhD Thesis

Barcelona, March 2012

Chapter 4.

RESULTS BLOCK I

ATP-Dependent Potassium Channel Blockade Strengthens Microglial Neuroprotection after Hypoxia-Ischemia in Rats

Ortega F.J., Gimeno-Bayon J., Espinosa-Parrilla J.F., Carrasco J.L., Batlle M., Pugliese M., Mahy N., Rodríguez M.J.

Exp Neurol (2012) Feb 24 (*Epub ahead of print*). doi: 10.1016/j.expneurol.2012.02.010

4.1 Summary

Stroke causes CNS injury associated with strong fast microglial activation as part of the inflammatory response. In rat models of stroke, sulfonylurea receptor blockade with glibenclamide reduced cerebral edema and infarct volume. We postulated that glibenclamide administered during the early stages of stroke might foster neuroprotective microglial activity through ATP-sensitive potassium (K_{ATP}) channel blockade. We found *in vitro* that BV2 cell line showed upregulated expression of K_{ATP} channel subunits in response to pro-inflammatory signals and that glibenclamide increases the reactive morphology of microglia, phagocytic capacity and TNFα release. Moreover, glibenclamide administered to rats 6, 12 and 24 hours after transient Middle Cerebral Artery occlusion improved neurological outcome and preserved neurons in the lesioned core three days after reperfusion. Immunohistochemistry with specific markers to neuron, astroglia, microglia and lymphocytes showed that resident amoeboid microglia are the main cell population in that necrotic zone. These reactive microglial cells express SUR1, SUR2B and Kir6.2 proteins that assemble in functional K_{ATP} channels. These findings provide that evidence for the key role of K_{ATP} channels in the control of microglial reactivity are consistent with a microglial effect of Glibenclamide into the ischemic brain and suggest a neuroprotective role of microglia in the early stages of stroke.

4.2 Introduction

ATP-sensitive potassium (K_{ATP}) channels are expressed by neurons of different brain regions (Ashford et al., 1990; Levin 2001; Ohno-Shosaku and Yamamoto 1992) and other cell types such as pancreatic β-cells (Aguilar-Bryan et al., 1995; Ashcroft et al., 1987), in which they act as energy sensors of ATP production. The expression of K_{ATP} channels has also been suggested in microglia (McLarnon et al., 2001, RAMONET2004; Ramonet et al., 2004). K_{ATP} channels are assembled as a hetero-octameric complex (Clement et al., 1997; Mikhailov et al., 2005; Proks and Ashcroft 2009; Wheeler et al., 2008) from two structurally distinct subunits: the regulatory sulfonylurea receptor (SUR), a member of the ATP-binding cassette protein family with 3 isoforms SUR1, SUR2A and SUR2B, and the pore forming inwardly rectifying

K^+ channel (Kir) subunit 6.1 or 6.2. Sulfonylureas such as glibenclamide (Gbc) close the channel by interaction with two drug-binding sites on SUR subunits (Mikhailov et al., 2001) and are used to treat diabetes.

In several rat models of stroke, blockade of SUR with low doses of Gbc reduced cerebral edema and infarct volume, and decreased mortality by 50% (Simard et al., 2010). These cytoprotective effects of Gbc are related to the astroglial $NC_{Ca\text{-}ATP}$ channel, whose activity is under SUR1 control (Chen et al., 2003). However, as SUR assembles with Kir6.x subunits to constitute functional K_{ATP} channels, other possible effects of Gbc might explain the effectiveness of this drug in the treatment of stroke.

Microglia generally considered the immune cells of the CNS (Graeber and Streit 2010; Kim and de Vellis 2005; Napoli and Neumann 2009), normally monitors brain environment and synapse functional status (Wake et al., 2009). After injury, microglia adopt an amoeboid shape, show an upregulated variety of surface molecules and release of cytokines. Excessive production of pro-inflammatory and neurotoxic factors from activated microglia, such as nitric oxide (NO), tumor necrosis factor a (TNFα), interleukin-1β and reactive oxygen species, may trigger or exacerbate neuronal death (Acarin et al., 2000). However considerable evidence after ischemia shows that microglial response caused by injured/dying neurons mediates a reduction of neuronal damage and induction of tissue repair (Kitamura et al., 2004; Lalancette-Hébert et al., 2007; Neumann et al., 2006; Neumann et al., 2008; Shaked et al., 2005; Streit 2002; Thored et al., 2009). For example, experimental transient astroglial ablation in the hippocampus and other brain regions is associated with a protective microglial reaction that avoids any neuronal injury over several days (Rodriguez et al., 2004). Consequently, in pathological processes microglia show a hybrid activation state that includes inflammatory actions and also characteristics of neuroprotection and repair (Hanisch and Kettenmann 2007; Milligan and Watkins 2009; Streit 2005; Thored et al., 2009). In any case, in response to neuronal damage fast activation of microglia requires the rapid availability of a large amount of energy to trigger diverse cytotoxic or neuroprotective signals. The expression of K_{ATP} channels in activated microglia, coupling cell energy to membrane potential may then be critical in determining, at least in part, their participation in the pathogenic process.

If this is the case, Gbc effects in stroke should include strengthening of neuroprotective microglial activity. We studied the effects of Gbc on microglial inflammatory and phagocytic activities in cultures of the BV2 microglial cell line and then, investigated this possibility in the transient middle cerebral artery occlusion (tMCAo) rat stroke model, by a combined functional, imaging, histological and stereological approach. We report that once activated, microglia upregulate the expression of K_{ATP} channels and blockade of the channel by Gbc fosters the neuroprotective activity of microglia in the early stages of injury, which facilitates major improvements in stroke outcome.

4.3 Material and Methods

To assess the presence of the K_{ATP} channel components SUR1, Kir6.1 and Kir6.2 on microglial cells, we used the murine BV2 cell line. Cell cultures undergo reactive by stimulation with 0.1 mg/mL of LPS and 0.05 ng/mL of IFNγ for 48h, after when we collected the cellular fraction as well as the culture media. From the cellular fraction (n = 3), we performed RT-PCR to detect mRNA and western-blotting from the whole-cell culture to detect the protein fraction. We Immunodetection of the K_{ATP} channel components on coverslips were used to visualize the protein expression directly on the cells.

To analyze whether Gbc modifies cellular physiology (n= 6), we activated the cells as described above but in absence or presence of Gbc (1 nM, 10^{-3} nM or 10^{-5} nM). Gbc was added to the cells 30 min prior to activation (Pre-treatment) or 24h post-activation (Post-treatment). After 48 h, cell morphology was analyzed by immunocytochemistry, and the phagocytic capacity 5, 10, 20 or 30 min in presence of FluoSpheres. Released factors such as TNFα or NO were quantified from the culture media.

Focal ischemia of 60 min was produced by tMCAO using the intraluminal filament technique (Van Groen et al., 2005). Sixty-three Wistar male rats were separated as follows:

- 3 pMCAO rats received an i.p. injection of 100 μCi [^{3}H]Gbc 16 h after ischemia onset.
- 15 tMCAO rats treated with vehicle (0.01 M PBS) i.v.

- 15 tMCAO rats treated with Gbc 0.02 µg i.v. 6, 12 and 24 h after the onset of reperfusion (Final dose of Gbc 0.06µg)
- 15 tMCAO rats treated with Gbc 0.2 µg i.v. 6, 12 and 24 h after the onset of reperfusion (Final dose of Gbc 0.6µg)
- 15 tMCAO rats treated with Gbc 2 µg i.v. 6, 12 and 24 h after the onset of reperfusion (Final dose of Gbc 6µg)

Bioavailability of Gbc on ischemic animals, was measured by the specific ^{3}H emission two hours after the injection of [^{3}H]Gbc i.p.

We assessed the post-ischemic motor function and behavioral recovery of the tMCAO animals using the 7-point and 28-point neuroscore tests at: pre-MCAO (baseline), 2, 24, 48 and 72 h after reperfusion (3 day follow-up groups). To quantify lesion volume, animals were deeply anesthetized 72 h after reperfusion, and T_2-MRI was performed. After that, animals were sacrificed for histological and inmmunohistochemical analysis. Sections stained with Haematoxylin-Eosin (H&E) were randomly selected to determine the total infarct volume whereas degenerating neurons were detected by Fluorojade B staining. To determine calcium deposits, sections were stained with the Alizarin red method and counterstained with fast green solution.

Were measured the areas of astrogliosis and microgliosis on GFAP-immunostained and IB4-stained sections. Moreover, stereological methods were used to quantify the number of neurons (NeuN) and astrocytes (GFAP) at the core of the lesion (-0.8 to -1.8 of bregma).

To detect the K_{ATP} channel components SUR1, SUR2B and Kir6.2 on microglial cells *in vivo*, we performed double immunofluorescence labeling using specific antibodies against the channel components and microglia (CD11b) into tMCAO samples.

4.4 Results

4.4.1 BV2 cell activation with LPS+IFNγ enhances K_{ATP} channel expression

To investigate the direct Gbc effects on microglia, we activated and treated with Gbc murine BV2 microglia. We first assessed by RT-PCR the expression of SUR1, SUR2A, SUR2B, Kir6.1 and Kir6.2, before and after activation with LPS+IFNγ. Here

we used total RNA from murine pancreas and lung, which constitutively express K_{ATP} channels, as positive controls, and total RNA from HEK293 cells as negative control. After reverse transcription with oligo-dT primers and amplification, electrophoresis showed amplicons of the predicted size for SUR1, Kir6.1 and Kir6.2. (**Fig. 4.1A, E, I**). Amplicons for Kir6.1 and Kir6.2 were at higher quantities in BV2 cells activated with LPS+IFNγ than in non-activated cells. We could not reproduce SUR2A and SUR2B results because of the low amount of DNA from their amplicons, which was at the limit of detection of the technique (data not shown)

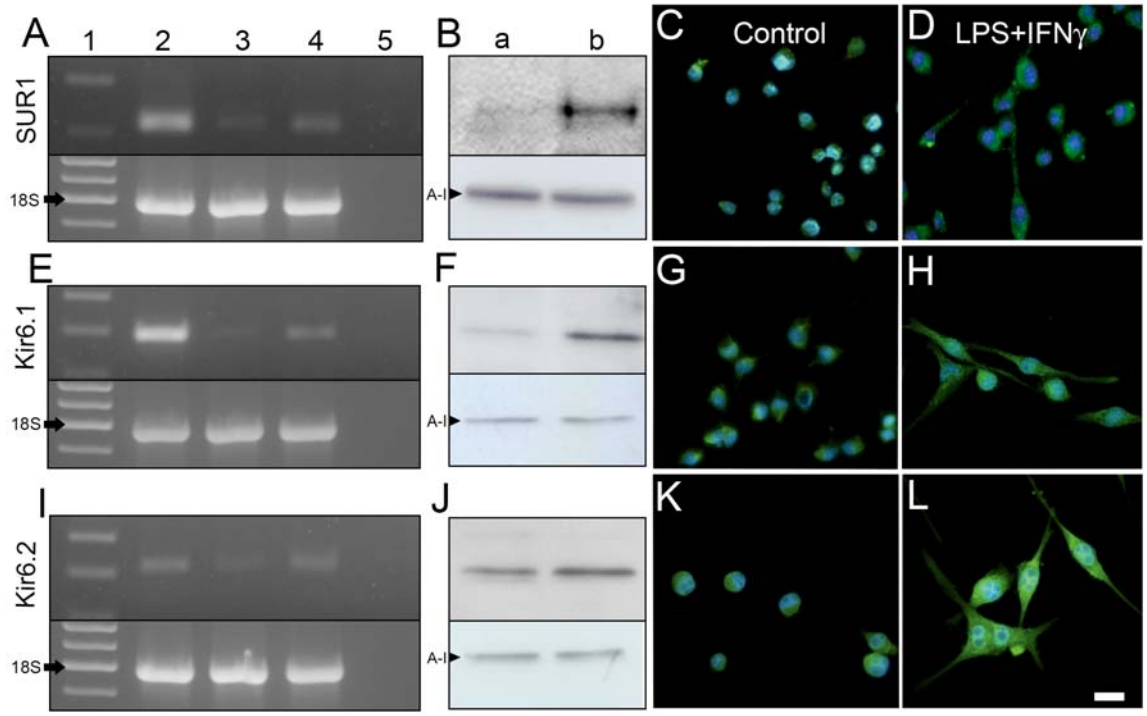

Fig. 4.1. BV2 microglial expression of K-$_{ATP}$ channel components. Murine BV2 cell culture was analyzed 48h after activation with LPS+IFNγ (see material and methods for details) **(A, E, I)** RT-PCR analyses of K-$_{ATP}$ channel subunits were performed with gene-specific primers (Table 1). PCR products for **(A)** SUR1, **(E)** Kir6.1 and **(I)** Kir6.2 and 18S as control of mRNA quantity in each reaction (arrows, 488bp) were separated by 1.5% agarose gel electrophoresis and stained with ethidium bromide. **(Line 1)** Each gel was loaded with standard size markers and **(Line 2)** cDNA amplified from: pancreas (SUR1 and Kir6.2) and lung (Kir6.1) as control; **Line 3**, non-activated BV2 cells; **Line 4**, BV2 cells activated with LPS+IFNγ; and **Line 5**, total RNA from HEK293 cells was used as negative controls. Amplified fragments had the sizes of 217bp for SUR1, 297pb for Kir6.1 and 312bp for Kir6.2 as predicted by the mRNA sequences amplicons. **(B, F, J)** Immunoblots of SUR1 **(B)**, Kir6.1 **(F)** and Kir6.2 **(J)** expressed by control **(Line a)** and activated **(Line b)** BV2 cells. Homogenates were normalized for protein content quantified by Bradford's method and 15 µg of protein was applied in each gel lane. Bands appeared at the level of 190kDa for SUR1, 50kDa for Kir6.1 and 40kDa for Kir6.2. Actin-I was thereafter blotted as control of protein quantity in each gel (arrowhead, 43kDa). Immunocytochemistry with specific antibodies against **(C, D)** SUR1, **(G, H)** Kir6.1 and **(K, L)** Kir6.2 was performed in control and BV2 cells activated with LPS+IFNγ. Specific binding was detected with AlexaFluor 488-conjugated secondary antibodies (green). Cell nuclei were counterstained with Hoescht33258 (blue). Note that activated BV2 cells are bigger and showed numerous processes. (n= 3 different cultures). Scale Bar 20 µm.

We then quantified the relative protein concentration of the channel components by Western-blot. We found specific bands for SUR1, Kir6.1 and Kir6.2 proteins at predicted sizes. When quantified, all three proteins had higher concentrations 48h hours after LPS+IFNγ activation, with a 5.21-fold increase for SUR1, 3.26-fold for Kir6.1, and 1.38-fold for Kir6.2 (**Fig. 4.1B, F, J)**. Immunocytochemistry confirmed these results. In control BV2 cells, all three proteins had a weak basal staining (**Fig. 4.1C, G, K)**. After activation both the number of cell processes and specific labeling of SUR1, Kir6.1 and Kir6.2 increased (**Fig. 4.1D, H, L**).

4.4.2 Gbc modifies activated BV2 microglial activity

We then investigated whether Gbc directly modulates NO and pro-inflammatory cytokine production in activated BV2 microglia. We added Gbc to the media at 3 different concentrations (1 nM, 10^{-3} nM or 10^{-5} nM) 30 min prior to activation (pre-treatment) or 24 hours after activation (post-treatment). At 48 hours LPS+IFNγ increased the NO production of BV2 cells 6-fold and Gbc did not modified this increase. Under these same conditions, LPS+IFNγ increased TNFα release in the medium ($t=-5.6$; $p<0.01$), which resulted 45% higher after pre-treatment with 10^{-5} nM Gbc ($F_{19,3}=3.49$; $p=0.04$). By contrast, Gbc 1 nM decreased TNFα release by quiescent BV2 cells ($t=-3.53$; $p=0.02$) (**Fig. 4.2A, B)**.

Activation of BV2 microglia involves a morphological change characterized spherical quiescent cells losing their spherical shape and the development of cell processes that are directly related to the phagocytic capacity of the cells. BV2 cell shape analysis performed 48 hours after incubation with LPS+IFNγ showed a higher perimeter/area ratio, which confirmed the activation state of the cells ($KS=2.7$; $p<0.01$). 10^{-5} nM and 10^{-3} nM Gbc pre-treatment induced an increase in the perimeter/area ratio values of activated cells ($KW=31.8$; $p<0.01$; **Fig. 4.2C, G**). Gbc post-treatment required higher concentrations to produce similar results (10^{-3} nM and 1 nM; $KW=50.6$; $p<0.01$) (**Fig. 4.2D)**.

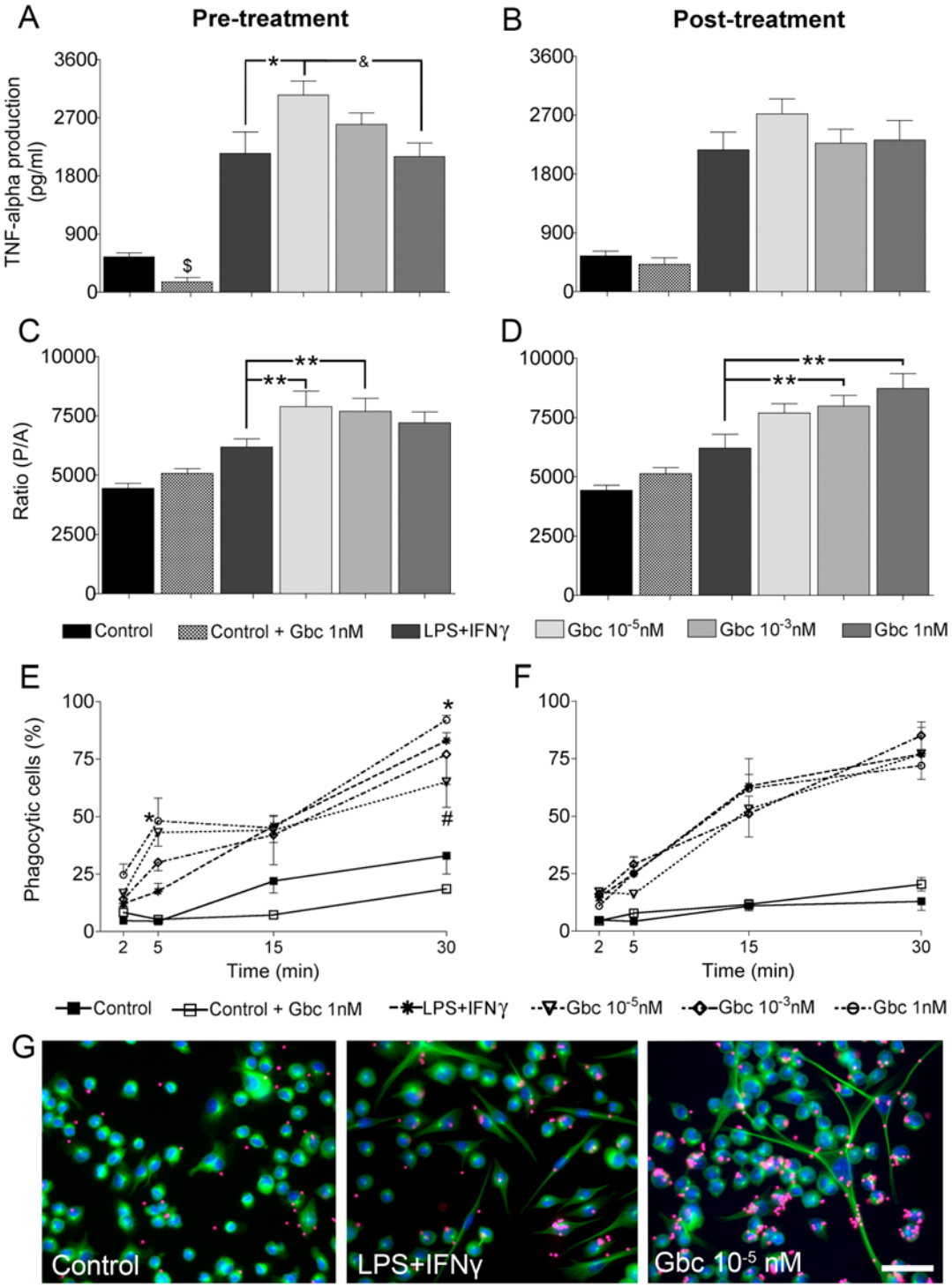

Fig. 4.2. BV2 cells are more reactive and phagocytic when are treated with Glibenclamide. (**A-F**) TNFα release, cell reactivity as morphology and phagocytic capacity of BV2 cells were assessed 48h after activation with LPS+IFNγ and pre-treated **(left column)** or post-treated **(right column)** with Gbc 10^{-5}nM, 10^{-3}nM or 1nM (n=7). Bar graph show: **(A-B)** TNFα release quantified by ELISA and **(C-D)** reactive phenotype quantified as a perimeter/area ratio. (**E-F)** Graph shows the quantification of time course of the BV2-cell phagocytic capacity measured by fluosphere assay (%). (**G**) Illustrative photomicrographs of BV2 cells during fluosphere assay after 5 min in presence of the beads (**red**). Cells were labeled with anti-tubulin (**green**) and DAPI (**blue**). Note that cells pre-treated with Gbc 10^{-5} nM increased their phagocytic capacity and present more and longer processes, therefore increasing the ratio perimeter/area. All values are presented as mean ±SEM (n= 6 different cultures). Statistics: In **(A-D)** **P*<0.05, ***P*<0.01 vs LPS+IFNg; $^{\&}P$<0.05 vs other Gbc doses; $^{\$}P$<0.05 vs Control. In **(E-F)** **P*<0.05 vs LPS+IFNγ; $^{\#}P$<0.05 different from all the other groups. Scale bar 25 µm.

Finally, we quantified the phagocytic capacity of activated BV2 microglia. 48 hours after activation the percentage of phagocytic cells increased 2, 5, 15 and 30 min after incubation in presence of fluosphere (KW=7; $p<0.01$). Five minutes after fluosphere incubation, Gbc pre-treatment increased the percentage of phagocytic cells ($F_{11,3}=6.20$; $p=0.01$; **Fig. 4.2E, F)**. At this time point, 10^{-5} nM and 1 nM Gbc both increased the percentage of phagocytic cells, but 1 nM Gbc produced the maximal effect which remained stable during the 30 minutes of the study. In contrast, Gbc post-treatment did not modify the phagocytic capacity at any dose (**Fig. 4.2G).**

4.4.3 Gbc improves the neurological outcome of tMCAO rats.

We injected [^{3}H]Gbc (100 µCi) i.p. to animals 16 hours after permanent MCAO to investigate whether Gbc enters the ischemic rat brain after peripheral administration. Two hours later, the specific [^{3}H]Gbc binding to the ischemic hemisphere was significantly greater than in the control hemisphere ($t=7.7$, $p=0.0014$), whereas the value of the uninjured hemisphere was similar to non-radioactive tissue ($t=3.445$; $p=0.0749$; **(Fig. 4.3A)**. Only 0.025% of injected [^{3}H]Gbc entered the control brain, but permanent MCAO-induced blood-brain barrier breakdown increased this value to 0.077%, which resulted in binding values similar to those of heart and kidney (data not shown). Thus, peripherally administered Gbc reaches the ischemic brain, where it could have a specific pharmacological effect.

To assess whether Gbc improves the motor and behavioral recovery after stroke, 4 groups of 60 min tMCAo animals received 0 µg (vehicle group), 0.06µg, 0.6µg and 6µg Gbc. Then, we conducted double-blind 7-point and 28-point neuroscore tests in all animals at the following times: pre-tMCAo (baseline), 2 h, 24 h, 48 h and 72 h after reperfusion. We found an overall reduction of 7-point neuroscore test values 2h after the occlusion. When compared with the vehicle group, none of the Gbc-treated groups improved the 7-point neuroscore values at any time point. However, when we analyzed data of each group as a time-course, we detected a 25% score improvement at 72 h in the 0.6µg Gbc-treated animals, compared with the 24 h time point ($t=3.65$, $p=0.0076$; **Fig. 4.3B)**.

We also found an overall reduction of the 28-point test values 2h after the occlusion and, compared with vehicle, Gbc treatments did not improved those

values at any time-point. Vehicle, 0.06µg, 0.6µg and 6µg Gbc-treated animals improved their score at 72 h over their 24 h values (t=3.92, p=0.0097; t=3.89, p=0.0113; t=4.99, p=0.0002, and t=3.83, p=0.0142 respectively). In animals treated with 0.6µg Gbc, this recovery was higher and already significant 48 h after tMCAo (t=3.64, p=0.0244, data not shown).

72 h after tMCAo, we identified brain damage and quantified cortical, subcortical and total infarct volumes by T_2-MRI, to determine whether this Gbc-induced motor recovery is connected with a reduction of brain lesion **(Fig. 4.3C, D)**. None of the doses of Gbc modified these volumes when compared with the vehicle group. Under our experimental conditions, MRI did not allowed to discrimination between the peri-infarcted and necrotic zones within the lesion volume, and we could not perform accurate quantification of these volumes due to the limitations of the technique. We then investigated the putative neuroprotective effect of Gbc in the tMCAo lesion through a histological approach.

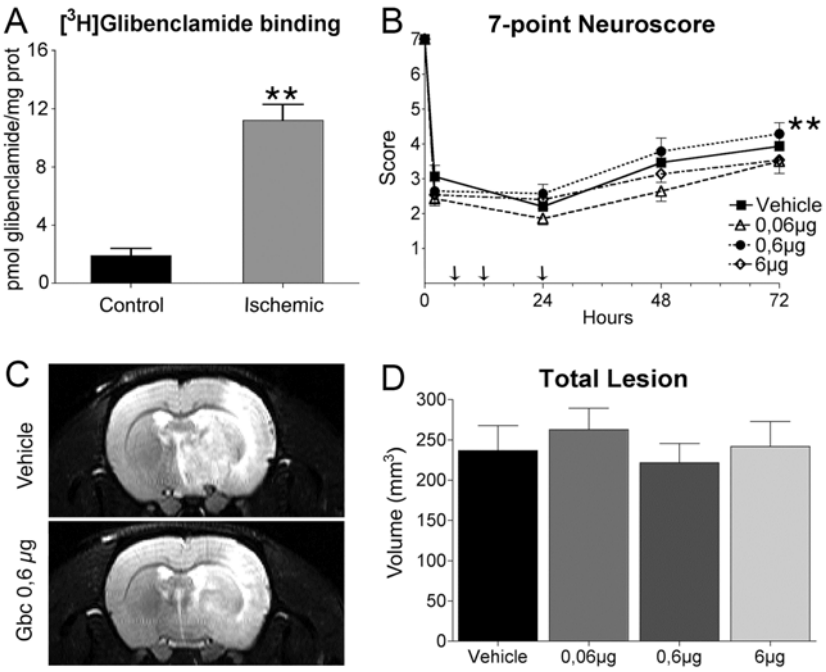

Fig. 4.3. Gbc reaches the ischemic brain and improves the neurological outcome of tMCAO animals. **(A)** Specific [^{3}H]Gbc binding in control and ischemic brain. **(B)** Timing of the 7-point Neuroscore values presented by tMCAO animals in a dose response study of three Gbc doses (0.06µg, 0.6µg and 6µg) and vehicle; arrows indicate the time of Gbc i.v. administration, see material and methods for details. (**C)** Representative T2-MRI image 72 h after tMCAO in vehicle and 0.06µg Gbc-treated animals. **(D)** Bar graph of total lesion volumes calculated from MRI data of all animals included in the dose response study. Results are represented separately as Mean (±SEM) for all the groups (n= 15 rats/group). Statistics: ***P*<0.01 different from control in (A) and compared with the 24 h time point in (B) (LSD post-hoc test).

4.4.4 Glibenclamide decreases tMCAO-induced neuronal loss and brain calcification

According to MRI results, the whole ischemic lesion studied on H&E stained sections only showed a slight reduction, which did not reach significance with any dose of Gbc when compared with the vehicle group (**Fig. 4.4**). However, at the ischemic focus (from -0.8 to -1.8 mm to bregma; **Fig. 4.6A**) this slight reduction reflected significant changes of the peri-infarcted and the necrotic volumes as described below.

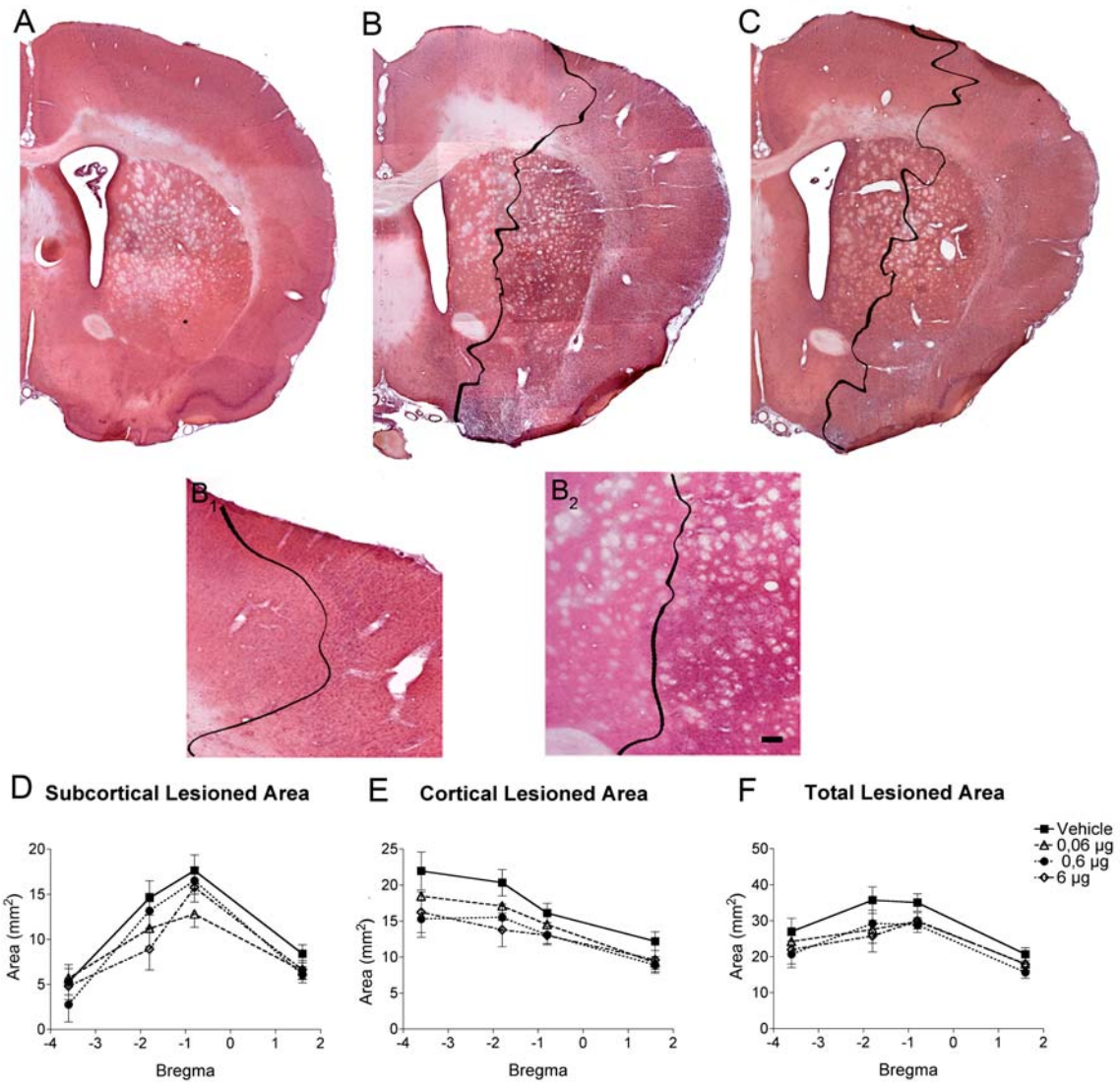

Fig. 4.4. Haematoxylin-Eosin staining images of the ipsilateral hemisphere from **(A)** control, **(B)** vehicle and **(C)** Gbc 0,6 µg treated brain. Higher magnification images from the vehicle animal, which show the boundary of the lesions in the cortex (B_1) or the striatum (B_2). Graphical representation of the cortical **(D),** subcortical **(E)** and the total lesioned area **(F)** along the bregma axis. Note that although not statistical differences were found, treated groups had lower values for lesioned areas in all bregma levels studied. Scale bar 200 µm.

Detailed analysis of the total necrotic volume examined by Neu-N immunohistochemistry, defined as the volume lacking Neu-N-positive cells, showed differences between treated groups **(Fig. 4.5A-D)**.

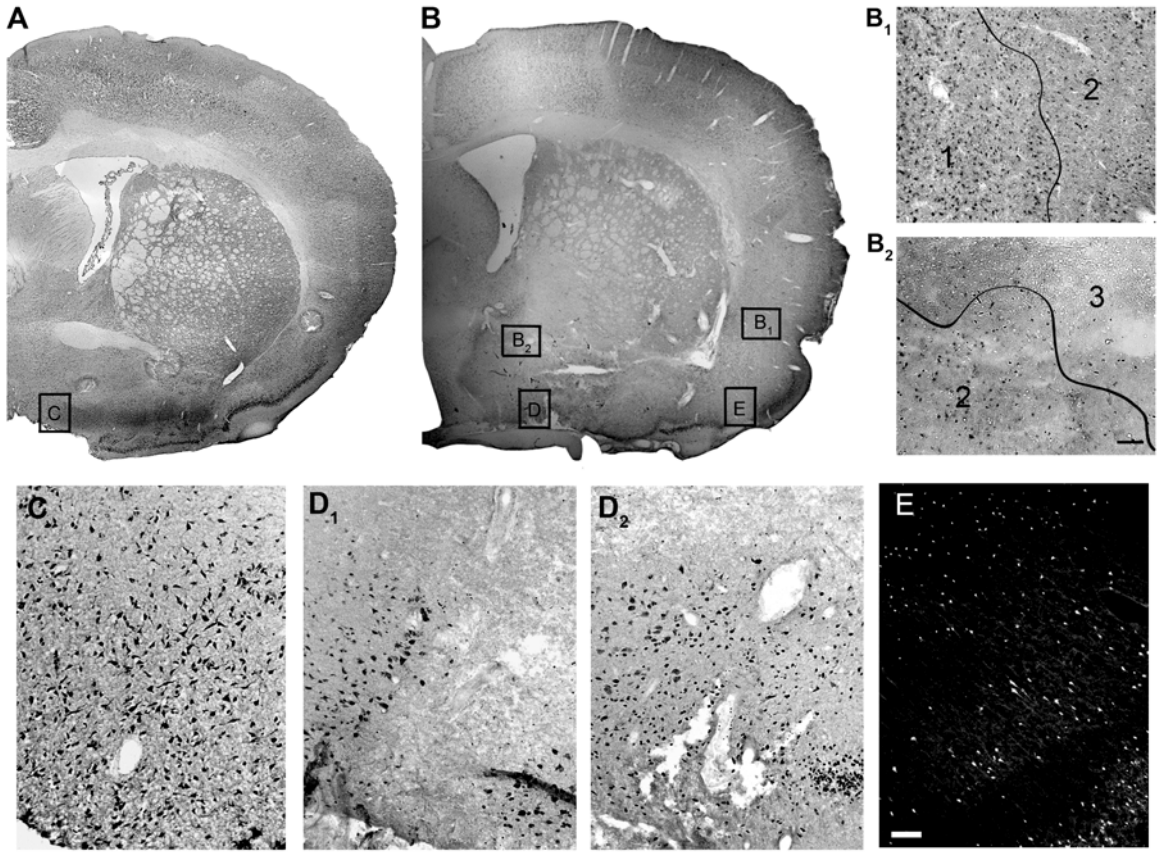

Fig. 4.5. Glibenclamide causes neuroprotection in ischemic brains. Representative NeuN immunostaining: **(A)** control brain and **(B)** tMCAo brain, both on the ischemic core level (Bregma from -0,8 to -1.8). **(B_1, B_2)** Analysis at higher magnification of infarcted brain evidenced 3 different regions**:** healthy and organized tissue (1), peri-infarcted region with a decreased number of neurons and tissue disorganization (2), and a necrotic zone with few scattered NeuN-positive cells and more tissue disorganization (3). The effects of three Gbc doses (0.06µg, 0.6µg and 6µg) were compared to vehicle administration by a histological approach. Quantification of the lesioned, necrotic and peri-infarcted volumes and neuronal counts was made at the ischemic core by stereology. Photomicrographs of the Ventral Pallidum nuclei (**C**), which corresponds with the boundary between the necrotic core and peri-infarct area for a vehicle-treated (**D_1**) or for a Gbc 0.6µg treated animals (**D_2**). Note that in Gbc 0.6µg treated animals (**D_2**) the necrotic area is smaller and more NeuN-positive cells are observed in the boundary. **(E)** Photomicrograph of degenerating neurons stained with FluoroJade B (FJB) in the peri-infarcted cortex of tMCAo animals. Scale bar 50 µm.

Dose of Gbc of 0.6 µg reduced the total necrotic volume compared with 0.06 µg Gbc and vehicle, whereas 6 µg Gbc only had differences compared with vehicle ($F_{38,3}$= 5,54; p=0.0035) **(Fig. 4.6B)**. At the cortical level, Gbc 0.6 µg and 6 µg decreased

the necrotic volume compared with vehicle ($F_{38,3}$=2.91; p=0.0480), whereas at the subcortical level only 0.6 µg Gbc reduced this volume ($F_{38,3}$=4,7; p=0.0079). This lack of modification of the whole ischemic lesion and this small decrease in necrotic volume imply an increase in the peri-infarcted volume, which resulted significant in the 0.6 µg and 6 µg Gbc groups ($F_{38,3}$=8.19; p=0.0003) **(Fig. 4.6C)**.

To express the Gbc effects in terms of neuronal loss, we performed stereological counting on these sections. Although cell density not changed, we found a slight tendency to reduction of neuron numbers in the necrotic zone of all Gbc-treated groups ($F_{43,3}$=4,72; p=0.073) **(Fig. 4.6E)**. Moreover, we observed a significant neuronal preservation in the subcortical peri-infarct zone in the 0.6 µg and 6 µg Gbc animals ($F_{43,3}$=8,01; p=0.0038) **(Fig. 4.6D)**. The same was true when the necrotic and peri-infarcted zones were taken together as a total lesion volume. In this case, 0.6 µg Gbc preserved more neuronal cells in the subcortical region than in the vehicle group and 0.06 µg dose, while 6 µg Gbc also showed greater neuronal preservation than the 0.06 µg dose ($F_{39,3}$=5.3; p=0.0041; $F_{35,3}$=5.13; p=0.0048) **(Fig. 4.6F)**.

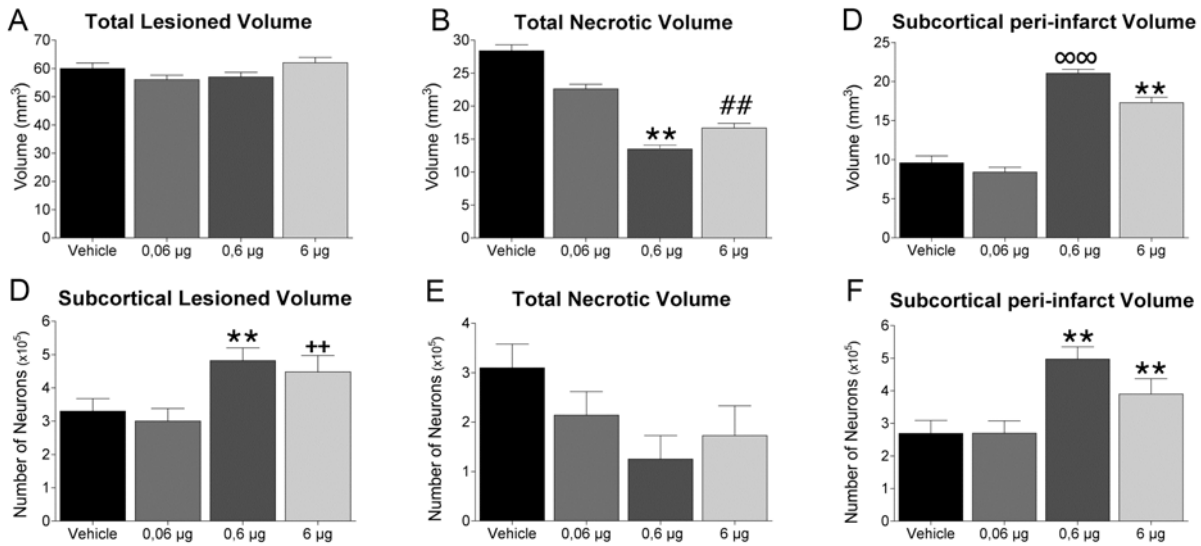

Fig. 4.6. Bar graphs of the **(A)** total lesioned, **(B)** total necrotic and **(C)** subcortical peri-infarcted volumes are shown together with stereological counting of NeuN-positive cells into the **(D)** subcortical lesion, **(E)** total necrotic and **(F)** subcortical peri-infarcted zones. Note that Gbc increases peri-infarcted volume and neuronal preservation into the subcortical region. This resulted in a 30-40% preservation of neurons in the total lesioned hemisphere, since no Gbc cortical effects were observed (data not shown). Values are presented as mean (±SEM) for all the groups (n= 15 rats/group). Statistics: $^{\#\#}$ P<0.01 different from vehicle; ^{++}P<0.01 different from Gbc 0.06 µg; **p<0.01 different from vehicle and 0.06 µg; $^{\infty\infty}P$<0.01 different from all.

We then used FJB staining to evaluate neuronal suffering and the intensity of the neurodegenerative process. In the ischemic focus (-0.8 mm to bregma) of all tMCAo animals, we observed an intense FJB labeling of the cell body in several neurons of cortical and subcortical zones, particularly in the peri-infarcted zone **(Fig. 4.5G),** with no clear effect of Gbc on this FJB staining pattern.

Formation of insoluble calcium phosphate complexes is strongly linked to stroke-induced calcium dyshomeostasis and neuronal loss. Thus, we studied by Alizarin red staining whether Gbc modifies the tMCAo-induced calcification at ischemic core level **(Fig. 4.7A)**. Gbc treatment induced a reduction of the calcium deposit diameter in the 0.6 µg Gbc group *vs* vehicle and 0.06 µg Gbc group (KW=18.18; p=0.0004; **Fig. 4.7B)**. Gbc also decreased the calcium deposit number in a dose-dependent response that was significant in the cortical zone, reaching statistical significance at Gbc doses of 0.6 µg and 6 µg (KW=10.43; p=0.015; **Fig. 4.7A, C).** Thus, although Gbc did not modify neurodegeneration, it fosters a neuronal preservation in the ischemic core and decreases calcification. This suggests that, once the injury processes are controlled, more neurons will be preserved in the peri-infarcted zone of Gbc-treated animals.

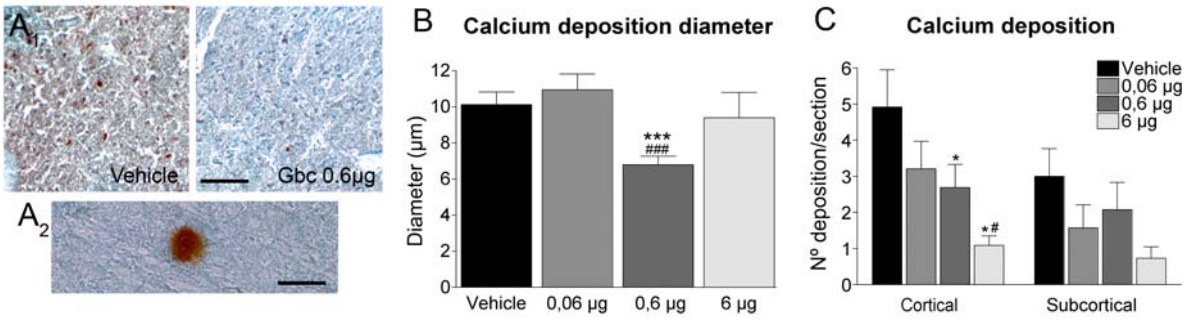

Fig. 4.7. Ischemic brain showed calcification. **(A)** Calcium deposition in the subcortical zone stained with 2% Alizarin red S counterstained with 0.5% Fast Green. The effects in calcification of three Gbc doses (0.06µg, 0.6µg and 6µg) compared with vehicle were studied in cortical and subcortical brain regions. (**A_1**) Images from a vehicle- and Gbc-treated animals. (**A_2**) High magnification photomicrograph of a single calcium deposit. Histograms show **(B)** the diameter size average of deposits and **(C)** the total number of calcium deposits per section (n= 15 rats/group). All values are presented as mean ±SEM. $^{*}P<0.05$ and $^{***}P<0.001$ different from vehicle; $^{\#}P<0.05$ and $^{\#\#\#}P<0.001$ different from Gbc 0,06µg; Scale Bar: (A_1) 150 µm; (A_2) 10 µm.

4.4.5 Glibenclamide does not modify tMCAO-inducible astrogliosis

We then studied the astroglial reaction associated with tMCAo in the ischemic focus by GFAP and S100β immunohistochemistry. GFAP immunohistochemistry revealed astrocytes with hypertrophy and hyperplasia, as well as high GFAP immunostaining covering almost the whole lesioned hemisphere. However, we found zones lacking astrocyte labeling coincident with the cortical and subcortical necrotic zones defined by NeuN immunohistochemistry **(Fig. 4.8A, B),** and their quantification showed no difference between groups (data not shown). In addition, Gbc did not modify tMCAo-induced astrogliosis or astrocyte density **(Fig. 4.8C)**.

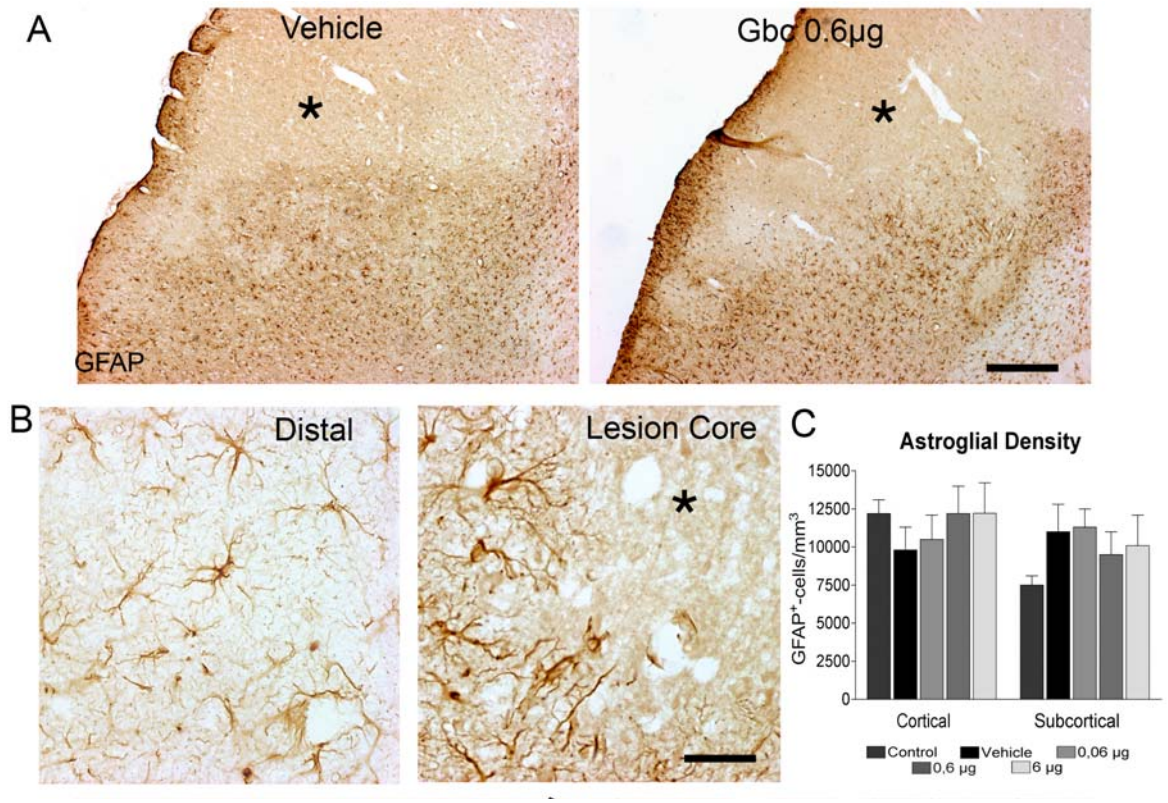

Fig. 4.8. Analysis of astroglial reactivity to tMCAO. **(A, B)** We visualized astrocyte distribution by GFAP immunohistochemistry in the entire tMCAO hemisphere and an area lacking specific GFAP immunostaining was found close to the astroglial scar (Asterisk), coincident with the lesion core. These areas were measured individually in the cortical and subcortical regions and pooled as total area, which value was not modified by Gbc treatment (data not shown). Non-reactive astrocytes were found in distal regions from the lesion. **(C)** Bar graph shows the astrocyte cell density quantified individually in each brain region of control (n= 4), vehicle (n= 15) and Gbc-treated brains (0.06µg, 0.6µg and 6µg; n= 15 rats/group). Values are presented as mean ±SEM. Scale Bar, 300µm in (A) and 20 µm in (B**)**.

S100β immunohistochemistry showed widespread S100β distribution around the necrotic zone, with the most intense immunoreactivity located in astrocytes of the corpus callosum and other areas of the white matter, in which Gbc increased S100β immunostaining and astrocyte hyperplasia **(Fig. 4.9)**.

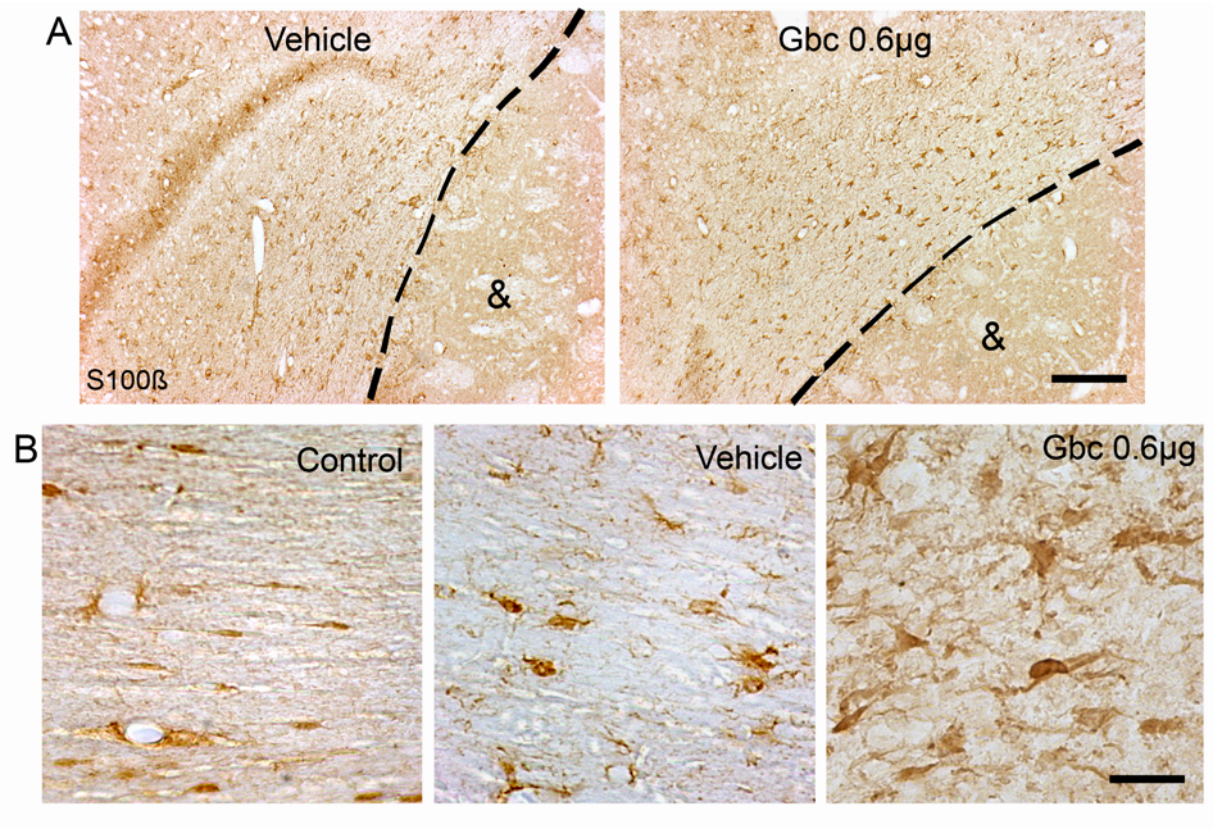

Fig. 4.9. (A) Illustrative S100β immunostainings images of the corpus callosum from the injured hemispheres (&; labels for Striatum). **(B)** Higher magnification images where: control brain showed organized tissue and small S100β cells with processes following the axons; tMCAO lesion caused tissue disorganization and increase S100β immunoreactivity and in the Gbc-treated tMCAO groups S100β positive cells presented major body volumes and higher number of processes. Scale bar, 150µm in (A) and 20 µm in (B).

4.4.6 Reactive microglia express K_{ATP} channels in tMCAO rat brain

We performed double immunolabeling and confocal microscopy at the ischemic core level (-0.8 mm to bregma) and used the CD3 antibody to detect T lymphocyte infiltration together with IB4, which stains microglia/macrophages **(Fig. 4.10B).** Within the necrotic core of some animals we detected small areas with few CD3-immunopositive cells, which never co-located with any IB4 staining. Thus, although CD3-immunopositive and IB4-positive cells showed tight contacts suggesting a

neuroimmune crosstalk as a response to the lesion, lymphocyte infiltration 3 days after tMCAo was small and did not interfere with IB4 labeling.

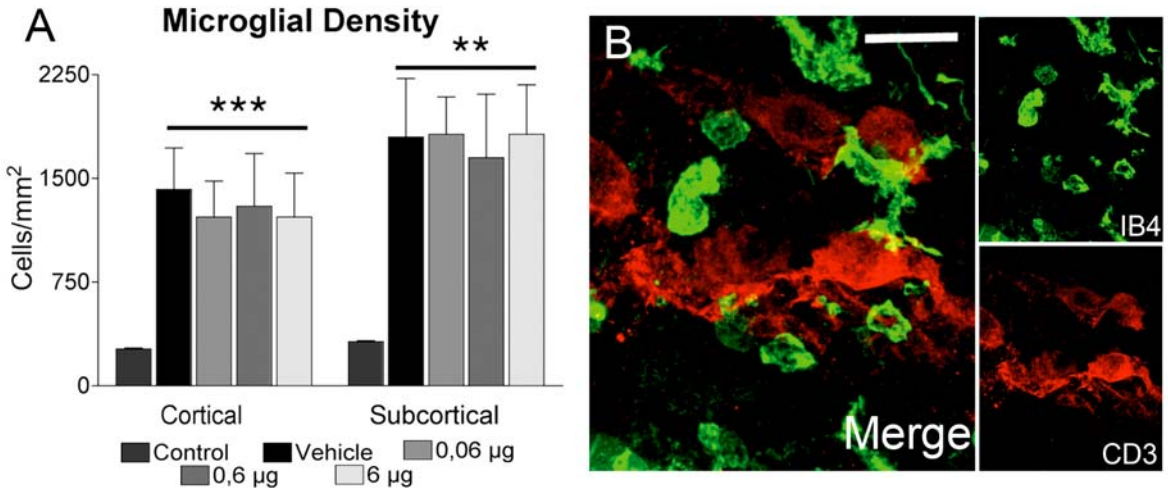

Fig. 4.10. T-lymphocytes infiltration. **(A)** Histogram shows microglial density determined individually in each brain region of control, vehicle and Gbc-treated brains (0.06µg, 0.6µg and 6µg). Ischemia triggers an increase of microglial density compared with control brain. **(B)** Illustrative confocal microscopy image of CD3-immunostained T-lymphocyte (CD3) infiltration in the infarct core, where IB4 positive microglia/macrophages (IB4) were reactive**.** Note that merged image shows both type of cells with tight contacts, suggesting a neuro-immune crosstalk as a response to the lesion**.** Values are presented as mean ±SEM (n= 15 rats/group). Statistics: ***P*<0.01 and ****P*<0.001 different from control. Scale bar 20µm

Low magnification photomicrographs from IB4 stained tMCAo samples showed continuity in microgliosis reaction, and we do not observed boundary between the necrotic core and peri-infarct region (**Fig. 4.11C, D**). Nonetheless, morphology of IB4-labeled cells changed with their location and proximity to the infarct core of the lesion. The small cell body and several ramifications of resting microglia in healthy tissue **(Fig. 4.11E)** changed progressively into a larger cell body and a more ramified reactive morphology with numerous processes in the peri-infarcted zone **(Fig. 4.11F**). In the area between the peri-infarcted and necrotic zones, positive cells had a mixed reactive-amoeboid morphology **(Fig. 4.11G)**. We observed fully amoeboid cells within the necrotic core **(Fig. 4.11H),** in which we found massive loss of neurons and absence of GFAP-immunopositive cells**.** Gbc treatment did not modify the size of the zone occupied by tMCAo-induced reactive cells. Nonetheless, when we analyzed cell density we found a significant overall group effect in the cortical

(t=19.2, p=0.0008) and subcortical (t=16.1, p=0.009) zones of tMCAo groups (**Fig. 4.10A),** but Gbc presented no effects.

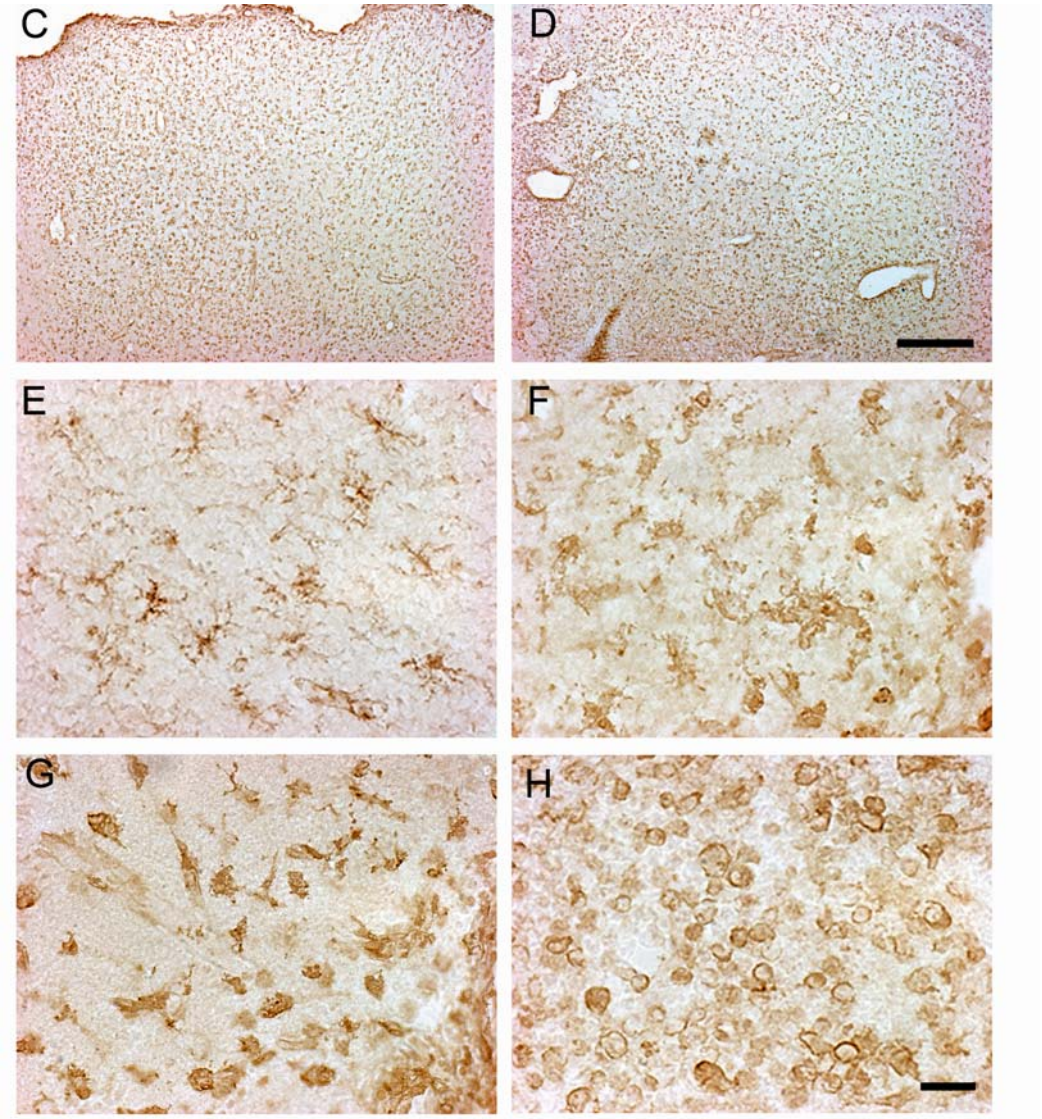

Fig. 4.11. Low magnification photomicrographs from (**C**) cortex and (**D**) caudate putamen, which shows continuity of the microgliosis reaction to the lesion. (**E-H**) Higher magnification photomicrographs showed variable microglial phenotype. **(E)** Resting microglial morphology was viewed in healthy tissue. **(F)** Reactive microglial cells were present in peri-infarcted areas and were more ramified than quiescent ones, with numerous processes. **(G)** Mixed morphology, some reactive and some amoeboid cells were detected in the border between peri-infarcted and necrotic areas. **(H)** Fully amoeboid shaped morphology cells were viewed in the necrotic core. Scale Bar, 300 µm in (D) and 20 µm in (B, H)**.**

To locate the cell expression of K_{ATP} channel components, we performed double immunohistochemical labeling with anti-SUR1, anti-SUR2B, or anti-Kir6.2 antibodies combined with anti-CD11b antibody as microglia/macrophage marker, with anti-NeuN as neuronal marker and with anti-GFAP as astroglial marker. Co-location

with anti-CD11b antibody indicated that reactive microglia within the necrotic zone expressed Kir6.2 (32.7±2.5%), SUR1 (40±2.7%) and/or SUR2B (39±7.5%) **(Fig. 4.12)**. Anti-SUR1 and anti-SUR2B antibodies also labeled some hippocampal and hypothalamic neurons and some astrocytes in the peri-infarcted zone, whereas Kir6.2 labeling did not clearly co-locate with GFAP immunolabeling in the ischemic brain (raw data not shown).

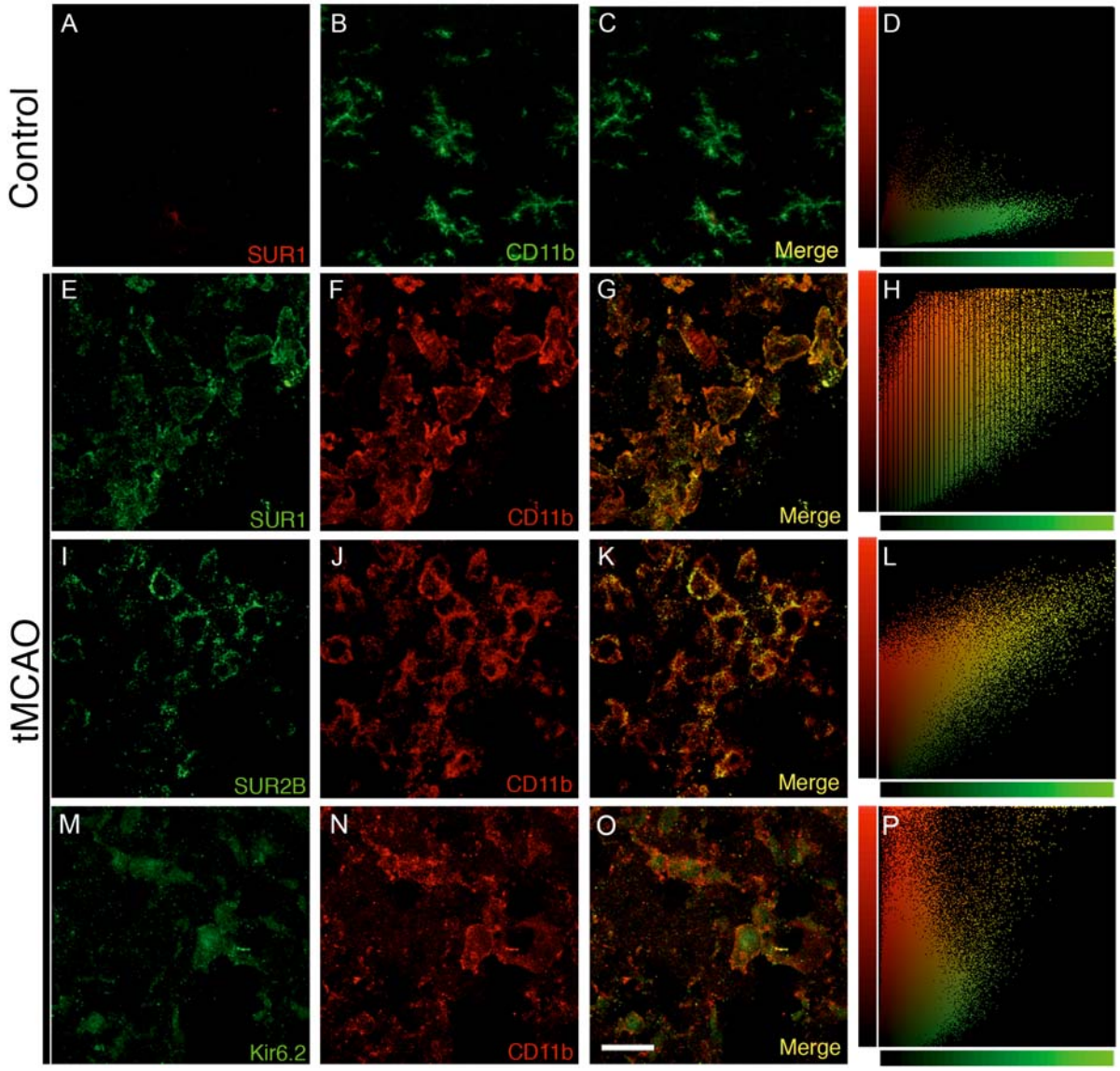

Fig. 4.12. Expression of K_{ATP} channel components SUR1, SUR2B and Kir6.2 in activated CD11b-positive cells into the core of the lesion (Bregma -0,8). **(A-D)** Confocal photomicrographs of SUR1 in resting microglia from control animals denote no colocalization. Reactive CD11b-positive cells expressed **(E-H)** SUR1, **(I-L)** SUR2B and (**M-P**) Kir6.2 channel subunits in the lesion core. (**D, H, L, P)** show scatter plots from its correspondent merged images from each row of the K_{ATP} channel components in reactive CD11b-positive cells. From left to right in the X-axis corresponds with the increase of the green channel intensity, whereas, from down to up in the Y-axis corresponds with the increase of the red channel. Yellow dots denote colocalization for both channels, in which CD11b-postive cells expressed SUR1 (**D, H**), SUR2B (**L**) and Kir6.2 (**P**). Scale Bar, 20 µm.

4.5 Discussion

In this study we identified the K_{ATP} channel as a key player in controlling microglia-mediated neuroprotection in focal cerebral ischemia. In our *in vitro* experiments we demonstrated that K_{ATP} channel subunit expression upregulated after LPS+IFNγ activation, and that its blockade increased reactive morphology, TNFα release and the phagocytic capacity of activated microglia. Furthermore, in the tMCAo rat model, we found that the improved neurological outcome and neuronal preservation in the necrotic core due to Gbc treatment did not correlated with the volume of lesion and astroglial reaction, and that resident amoeboid microglia are the main cell population in the necrotic zone. Also, reactive microglial cells express SUR1, SUR2B and Kir6.2 proteins that can assemble in functional K_{ATP} channels. Thus, K_{ATP} channels should directly participate in the control of microglial reactivity, with Gbc treatment resulting in a strengthening of the neuroprotective role of microglia/macrophages in the early stages of stroke. It is interesting to note that the Gbc doses used here are substantially lower than the ones used in previous studies presenting neuroprotective effects (Simard et al., 2009).

In our model of tMCAo, low doses of Gbc administered at 6, 12 and 24 hours after reperfusion reached the ischemic brain and significantly reduced the lesion's severity, as it improved motor neurological outcome and triggered neuronal preservation in the peri-infarcted region. Nonetheless, the volume of lesion measured by MRI did not reflect this Gbc-mediated neuroprotection. Most rodent models of stroke focus on the outcome measurement of lesion size in terms of infarct volume and brain edema. Within the first 3 days of lesion, the methodological approach and accuracy in these measurements are essential, since brain edema development may lead to overestimation of infarct volume (Lin et al., 1993). This accuracy reaches crucial importance in the assessment of drugs activity, since their neuroprotective effects may not be reflected by these two parameters (Walberer et al., 2010). Under our conditions, we used MRI to assess changes in the lesion's volume size, but this approach cannot give a precise indication of the severity of the injury (Simard et al., 2010) and is not accurate enough to measure the necrotic core of the lesion. When we included histological methods, measurement of the necrotic and peri-infarct zones (Lin et al., 1993) and neuronal counts defined the morphological

and cellular bases of the motor function improvement induced by K_{ATP} channel blockade.

The fate of the ischemic penumbra during the early steadies of the injury is considered the crucial element for stroke recovery (Furlan et al., 1996) since in the necrotic zone astrocytes and neurons are determined to die. The small size of the cerebral area occupied by CD3-immunopositive cells here observed for lymphocytes suggests little infiltration of blood cells 3 days after tMCAo. Moreover, infiltrated macrophages and granulocytes are proposed to not play major roles in the progression of ischemic neuronal damage for up to 16 hours, whereas reactive microglia are already detected in the zone from 6h post-tMCAo (Mabuchi et al., 2000). Furthermore, a transition of monocyte-derived cells into microglia is a very rare event that only occurs under highly defined host conditions (Mildner et al., 2007). Thus, microglial activity in the necrotic core would be crucial in determining the fate of the ischemic tissue. If true, the Gbc-induced neuronal preservation and functional recovery here found would reflect an enhancement of the neuroprotective microglial activity in the necrotic core.

Transcriptional upregulation of SUR1 in the ischemic brain is related to $NC_{Ca\text{-}ATP}$ channels of neurons, astrocytes and capillary endothelial cells of the peri-infarct region (Simard et al., 2006). As activation of $NC_{Ca\text{-}ATP}$ channels in astrocytes causes cell blebbing characteristic of cytotoxic edema, the Gbc-mediated reduction of infarct volume in permanent MCAO animals has been linked with blockade of these channels, whereas the involvement of K_{ATP} channels in the process has been ruled out (Simard et al., 2009). However, those studies did not assess the ischemia-induced expression changes of the trpm4 gene, the pore-forming subunit of $NC_{Ca\text{-}ATP}$ channels (Simard et al., 2010) and, despite the massive neuronal loss, immunoblots revealed no concentration changes of Kir6.1 and Kir6.2 proteins in the ischemic core (Simard et al., 2006). Our findings complete these results and argue for a contribution of K_{ATP} channels to the neuroprotective effects of Gbc by reducing the lesion's severity. Thus, we found that activation of microglia enhances SUR1, Kir6.1 and Kir6.2 protein expression, and that amoeboid microglia express K_{ATP} channels in the necrotic core of the lesion. This upregulation contributed to the enhancement of SUR1 found by Simard and cols. (2006), and helped compensate for a putative

decrease in Kir6.1 and Kir6.2 subunits due to the massive neuronal loss in the necrotic zone. It also explains the increased Kir6.1 and Kir6.2 expression in absence of the further neuronal damage in brain hypoxia described by other authors (Yamada et al., 2001).

Activation of K_{ATP} channels results in cell membrane hyperpolarization that may modulate microglial response to activation signals. Thus, the effects of an external stimulus on microglia are likely to be modulated at each moment by the number and degree of activated K_{ATP} channels, which in turn may depend, as in pancreatic β-cells, on the ATP/ADP cell ratio and ultimately on its energy level (Nichols 2006). Our findings reveal a direct influence of K_{ATP} channels on the phagocytic capacity and TNFα release of *in vitro* microglia, and also argue for Gbc enhancement of microglial reactivity in the early stages of stroke. Voltage- and calcium-dependent potassium channels participate in microglial functions, such as scavenging and neuroprotective actions (Eder 1998). As such, blockade of K^+ channels inhibits the respiratory burst and the morphological changes associated with *in vitro* microglial activation (Khanna et al., 2001). Here we provide evidence that Gbc increases the reactive morphology and phagocytic capacity of BV2 microglia activated with LPS+IFNγ. Microglial phagocytic abilities are essential for the clearance of cell debris and toxic compounds of the lesioned tissue, which underlies neuroprotection (Polazzi and Monti 2010). In addition, dying polymorphonuclear neutrophils (PMNs) infiltrated in the site of lesion, mediate neurotoxicity by the release of toxic intracellular compounds (Denes et al., 2007; Weston et al., 2007) and that, consequently, prompt phagocytosis of apoptotic PMNs by microglia might prevent the secretion of toxic compounds. Thus, clearance of PMNs from the nervous tissue might be an effective strategy to protect neurons from PMN neurotoxicity (Neumann et al., 2008). Also the K_{ATP} channel blockade slightly enhances neuronal loss in the necrotic core and these microglial cells are more efficient in clearing generated apoptotic cell debris, and reduces the secretion of pro-inflammatory cytokines (Magnus et al., 2001), and chemoattractants and T lymphocyte recruitment (Chan et al 2006). Overall, this data suggest that cell debris clearing will provide an optimal environment for neuroprotection in the surrounding tissue.

Furthermore, in hypoxia-ischemia, acute brain damage or excitotoxicity,

microglial reaction includes a phagocytic response to the formation of calcium deposits (Herrmann et al., 1998). Extension of calcification after hypoxia-ischemia in a brain area depends on the intensity of the acute phase and on the characteristics of each area of pathology (Lievens et al., 2000; Nonoda et al., 2009; Rodriguez et al., 2001). Here we found a Gbc-induced decrease in ischemic brain calcification with a reduced size and number of deposits, which represents a reduction in tMCAo-induced neuronal suffering and may be related to boosted microglial phagocytic activity.

Reactive microglial cells also release a broad panel of potentially neuroprotective factors. One of these factors is TNFα whose production reflects the complex roles of microglial activity with conflicting effects. We herein found that Gbc increases TNFα but does not increase NO release of BV2 microglia when activated with LPS+IFNγ. This result argues for a specific Gbc influence on TNFα release. TNFα secretion is crucial for autocrine fast microglial activation with cytotoxic effects. For example, microglial activation by aggregated β-amyloid or lipopolysaccharide increases TNFα secretion and renders them cytotoxic (Butovsky et al., 2005). However, in TNFα knock-out mice NO-mediated microglial activation appears delayed, results in further exacerbated non-specific microgliosis (Blais and Rivest 2004) and leads to the amplification of secondary excitotoxicity (Glezer et al., 2007). Actions of TNFα leading to neuronal death or survival are dose dependent (Bernardino et al., 2008), since it activates two specific receptors: TNFR1, with an intracellular death domain, and TNFR2 with higher affinity and mainly involved in neuroprotection (Fontaine et al., 2002). These two receptors are key elements in modulating neuronal sensitivity to ischemia, with microglial-derived TNFα being crucial to determining the survival of endangered neurons in the acute phase of focal cerebral ischemia (Lambertsen et al., 2009). Microglial TNFR2 is proposed to mediate the counter-regulatory response activated in neuropathological conditions (Veroni et al., 2010). In addition, TNFα is proposed as the molecular mediator of the microglial-mediated synapse removal, likely to be important in remodeling of neuronal circuits in the ischemic brain to ensure function (Wake et al., 2009) and involved in remyelination processes (Arnett et al., 2003). Consequently, TNFα actions leading to neuronal death or survival on neuronal damage are largely dependent on the context, timing, and dosage of TNFα

activity (Lenzlinger et al., 2001, Rolls 2008). Thus, often, a clear distinction between cytokines that are either harmful or beneficial cannot be established, since the primarily cytotoxic pro-inflammatory cytokines IL-1β and TNFα released from activated microglia may evoke a neuroprotective or pro-myelin regenerative response. For example, TNFα protects neurons against amyloid-beta-peptide-mediated toxicity (Barger et al., 1995) under pathological conditions, and has a role in homoeostatic synaptic scaling under physiological conditions (Stellwagen and Malenka 2006). In this regard, acute injury such as trauma or stroke activated microglia and their pro-inflammatory mediators may primarily have a neuroprotective role (Neumann et al., 2006) and therefore, anti-inflammatory treatment within the protective time window of microglia would be counterproductive.

Continuous crosstalk mediated by several signaling molecules, takes place between neurons, microglia and astrocytes, differently regulating their relationships in both health and disease (Polazzi and Monti 2010). In this regard, we here found a Gbc-induced increase of S100β in reactive astrocytes of the white mater, probably due to the $NC_{Ca\text{-}ATP}$ channel blockade (Simard et al., 2009), which may influence microglial-mediated neuroprotection. Released S100β modifies astrocytic, neuronal and microglial activities, whose effects depend on its extracellular concentration and the expression of the specific receptor RAGE. At micromolar concentrations, S100β upregulates TNFα expression in activated microglia (Bianchi et al., 2010). In addition, factors that modulate microglial reactivity, such as intracellular calcium concentration or TNFα, modify the RAGE response to S100β (Edwards and Robinson 2006) in a crosstalk that integrates these signaling systems. Thus, microglial reaction directly interacts with the concomitant astroglial reaction and the factors that determine this interaction, such as TNFα and S100β participate in the regulation of the activated phenotype of microglia after injury.

Finally, the peak of microglial activation occurs at seven days after stroke and remains activated for many weeks after tMCAo (Thored et al., 2009), with a dual role in the early and late stages of stroke (Neumann et al., 2006). Activated microglia can initially promote phagocytosis and brain regeneration, to then lose this protective phenotype when the injury progresses, with a persistent pro-inflammatory cytokine

production (Butovsky et al., 2005; Rolls et al., 2008). Thus, microglial activity enhancement induced by low doses of Gbc may anticipate the peak of activation and is probably transient, since Gbc boosts the microglial activity previous to the peak of activation and is metabolized within a few hours. If this were true, Gbc would foster the early microglial neuroprotective activity, but not the late cytotoxic one. To test this hypothesis, further experiments are necessary assessing the neuronal preservation and functional improvement of tMCAo rats at longer survival times.

In conclusion, the present findings demonstrate that Gbc improves functional neurological outcome in stroke, accompanied by neuron preservation in the core of the ischemic brain, and that the proposed stroke therapy aimed at SUR1 also involves microglial K_{ATP} channels. Moreover, the effects of Gbc on microglial activity identify K_{ATP} channels as a key target for modulating the neuroprotective role of microglia in the acute phase after focal cerebral ischemia. Therefore, our data clarify the mechanism of action of Gbc in stroke, and point out to microglia as a powerful regulator of neuronal survival. This also provides new therapeutic avenues for the treatment of other neurological disorders that involve microglia.

4.6 Acknowledgments

This research was supported by grants SAF2008-01902 and PET2007-0450 from the Ministerio de Ciencia e Innovación, and by grant 2009SGR1380 from the Generalitat de Catalunya (Autonomous Government), Spain. Neurotec Pharma also financed part of the study. F.J.O. holds a fellowship from Spanish Ministerio de Educación.

Contributions to the work: NM and MJR got financial support for the study; FJO, MP, NM and MJR designed the research study; FJO, JG-B, JFE-P and MB, performed the research, FJO, JLC, MP and MJR analyzed and discussed the data; FJO, NM & MJR wrote the paper.

4.7 Disclosures

M.P., N.M. and M.J.R. hold an EU patent (No. WO2006/000608) exploited by Neurotec Pharma. All three authors hold shares in Neurotec Pharma, M.P. is the

C.E.O. of the company and N.M. and M.J.R. are scientific advisors. The other authors report no disclosures.

4.8 References

Acarin L, Gonzalez B, Castellano B. 2000. Neuronal, astroglial and microglial cytokine expression after an excitotoxic lesion in the immature rat brain. Euro J Neurosc 12:3505-3520.

Aguilar-Bryan L, Nichols CG, Wechsler SW, Clement JP, Boyd AE, González G, Herrera-Sosa H, Nguy K, Bryan J, Nelson DA. 1995. Cloning of the beta cell high-affinity sulfonylurea receptor: a regulator of insulin secretion. Science 268(5209):423-6.

Arnett HA, Wang Y, Matsushima GK, Suzuki K, Ting JP-Y. 2003. Functional genomic analysis of remyelination reveals importance of inflammation in oligodendrocyte regeneration. J Neurosci 23(30):9824-32.

Ashcroft FM, Kakei M, Kelly RP, Sutton R. 1987. ATP-sensitive K+ channels in human isolated pancreatic β-cells. FEBS Lett 215(1):9-12.

Ashford ML, Boden PR, Treherne JM. 1990. Glucose-induced excitation of hypothalamic neurones is mediated by ATP-sensitive K+ channels. Pflugers Arch 415(4):479-83.

Barger SW, Van Eldik LJ, Mattson MP. 1995. S100β protects hippocampal neurons from damage induced by glucose deprivation. Brain Res 677(1):167-170.

Bernardino L, Agasse F, Silva B, Ferreira R, Grade S, Malva JO. 2008. Tumor necrosis factor-α modulates survival, proliferation, and neuronal differentiation in neonatal subventricular zone cell cultures. Stem Cells 26(9):2361-2371.

Bianchi R, Giambanco I, Donato R. 2010. S100B/RAGE-dependent activation of microglia via NF-kappaB and AP-1 Co-regulation of COX-2 expression by S100B, IL-1beta and TNF-alpha. Neurobiol Aging 31(4):665-77.

Blais V, Rivest S. 2004. Effects of TNF-α and IFN-γ on nitric oxide-induced neurotoxicity in the mouse brain. J Immunol 172(11):7043-52.

Butovsky O, Talpalar AE, Ben-Yaakov K, Schwartz M. 2005. Activation of microglia by aggregated beta-amyloid or lipopolysaccharide impairs MHC-II

expression and renders them cytotoxic whereas IFN-gamma and IL-4 render them protective. Mol Cell Neurosci 29(3):381-93.

Chen M, Dong Y, Simard JM. 2003. Functional coupling between sulfonylurea receptor type 1 and a nonselective cation channel in reactive astrocytes from adult rat brain. J Neurosci 23(24):8568-8577.

Clement JP, Kunjilwar K, Gonzalez G, Schwanstecher M, Panten U, Aguilar-Bryan L, Bryan J. 1997. Association and stoichiometry of K(ATP) channel subunits. Neuron 18(5):827-38.

Denes A, Vidyasagar R, Feng J, Narvainen J, McColl BW, Kauppinen RA, Allan SM. 2007. Proliferating resident microglia after focal cerebral ischaemia in mice. J Cereb Blood Flow Metab 27(12):1941-53.

Eder C. 1998. Ion channels in microglia (brain macrophages). Am J Physiol 275:C327-C342.

Edwards MM, Robinson SR. 2006. TNF alpha affects the expression of GFAP and S100B: implications for Alzheimer's disease. J Neural Transm 113(11):1709-15.

Fontaine V, Mohand-Said S, Hanoteau N, Fuchs C, Pfizenmaier K, Eisel U. 2002. Neurodegenerative and neuroprotective effects of tumor Necrosis factor (TNF) in retinal ischemia: opposite roles of TNF receptor 1 and TNF receptor 2. J Neurosci 22(7):RC216.

Furlan M, Marchal G, Viader F, Derlon JM, Baron JC. 1996. Spontaneous neurological recovery after stroke and the fate of the ischemic penumbra. Ann Neurol 40(2):216-26.

Glezer I, Simard AR, Rivest S. 2007. Neuroprotective role of the innate immune system by microglia. Neuroscience 147(4):867-883.

Graeber MB, Streit WJ. 2010. Microglia: biology and pathology. Acta Neuropathol 119(1):89-105.

Hanisch U, Kettenmann H. 2007. Microglia: active sensor and versatile effector cells in the normal and pathologic brain. Nat Neurosci 10(11):1387-94.

Herrmann G, Stünitz H, Nitsch C. 1998. Composition of ibotenic acid-induced calcifications in rat substantia nigra. Brain Res 786:205-214.

Khanna R, Roy L, Zhu X, Schlichter LC. 2001. K^+ channels and the microglial respiratory burst. Am J Physiol 280(4):C796-C806.

Kim SU, de Vellis J. 2005. Microglia in health and disease. J Neurosci Res 81(3):302-13.

Kitamura Y, Takata K, Inden M, Tsuchiya D, Yanagisawa D, Nakata J, Taniguchi T. 2004. Intracerebroventricular injection of microglia protects against focal brain ischemia. J Pharmacol Sci 94(2):203-6.

Lalancette-Hébert M, Gowing G, Simard A, Weng YC, Kriz J. 2007. Selective ablation of proliferating microglial cells exacerbates ischemic injury in the brain. J Neurosci 27(10):2596-605.

Lambertsen KL, Clausen BH, Babcock AA, Gregersen R, Fenger C, Nielsen HH, Haugaard LS, Wirenfeldt M, Nielsen M, Dagnaes-Hansen F and others. 2009. Microglia protect neurons against ischemia by synthesis of tumor necrosis factor. J Neurosci 29(5):1319-30.

Lenzlinger PM, Morganti-Kossmann MC, Laurer HL, McIntosh TK. 2001. The duality of the inflammatory response to traumatic brain injury. Mol Neurobiol 24(1-3):169-81.

Levin BE. 2001. Glucosensing neurons do more than just sense glucose. Int J Obes Relat Metab Dis 25(Supp 5):568-572.

Lievens JC, Bernal F, Forni C, Mahy N, Kerkerian-Le Goff L. 2000. Characterization of striatal lesions produced by glutamate uptake alteration: cell death, reactive gliosis, and changes in GLT1 and GADD45 mRNA expression. Glia 29(3):222-32.

Lin TN, He YY, Wu G, Khan M, Hsu CY. 1993. Effect of brain edema on infarct volume in a focal cerebral ischemia model in rats. Stroke 24(1):117-21.

Mabuchi T, Kitagawa K, Ohtsuki T, Kuwabara K, Yagita Y, Yanagihara T, Hori M, Matsumoto M. 2000. Contribution of microglia/macrophages to expansion of infarction and response of oligodendrocytes after focal cerebral ischemia in rats. Stroke 31(7):1735-43.

Magnus T, Chan A, Grauer O, Toyka KV, Gold R. 2001. Microglial phagocytosis of apoptotic inflammatory T cells leads to down-regulation of microglial immune activation. J Immunol 167(9):5004-10.

McLarnon JG, Franciosi S, Wang X, Bae JH, Choi HB, Kim SU. 2001. Acute actions of tumor necrosis factor-α on intracellular Ca^{2+} and K^+ currents in human microglia. Neuroscience 104(4):1175-84.

Mikhailov MV, Campbell JD, De Wet H, Shimomura K, Zadek B, Collins RF, Sansom MSP, Ford RC, Ashcroft FM. 2005. 3-D structural and functional characterization of the purified K_{ATP} channel complex Kir6.2-SUR1. EMBO J 24(23):4166-75.

Mikhailov MV, Mikhailova EA, Ashcroft SJ. 2001. Molecular structure of the glibenclamide binding site of the β-cell K_{ATP} channel. FEBS Lett 499(1-2):154-60.

Mildner A, Schmidt H, Nitsche M, Merkler D, Hanisch U-K, Mack M, Heikenwalder M, Brück W, Priller J, Prinz M. 2007. Microglia in the adult brain arise from Ly-6ChiCCR2$^+$ monocytes only under defined host conditions. Nat Neurosci 10(12):1544-53.

Milligan ED, Watkins LR. 2009. Pathological and protective roles of glia in chronic pain. Nat Rev Neurosci. p 23-36.

Napoli I, Neumann H. 2009. Microglial clearance function in health and disease. Neuroscience 158(3):1030-8.

Neumann J, Gunzer M, Gutzeit HO, Ullrich O, Reymann KG, Dinkel K. 2006. Microglia provide neuroprotection after ischemia. FASEB J 20(6):714-6.

Neumann J, Sauerzweig S, Rönicke R, Gunzer F, Dinkel K, Ullrich O, Gunzer M, Reymann KG. 2008. Microglia cells protect neurons by direct engulfment of invading neutrophil granulocytes: a new mechanism of CNS immune privilege. J Neurosci 28(23):5965-75.

Nichols CG. 2006. K_{ATP} channels as molecular sensors of cellular metabolism. Nature 440(7083):470-476.

Nonoda Y, Saito Y, Itoh M, Nakagawa E, Sugai K, Takahashi A, Otsuki T, Saito Y, Arima K, Mizuguchi M and others. 2009. Activation of microglia/macrophages expressing phosphorylated S6 ribosomal protein in a case of hemimegalencephaly with progressive calcification and atrophy. J Neurol Sci 287(1-2):52-9.

Ohno-Shosaku T, Yamamoto C. 1992. Identification of an ATP-sensitive K+ channel in rat cultured cortical neurons. Pflugers Arch 422(3):260-6.

Polazzi E, Monti B. 2010. Microglia and neuroprotection: from in vitro studies to therapeutic applications. Prog Neurobiol 92(3):293-315.

Proks P, Ashcroft FM. 2009. Modeling K_{ATP} channel gating and its regulation. Prog Biophys Mol Biol 99(1):7-19.

Ramonet D, Rodriguez MJ, Pugliese M, Mahy N. 2004. Putative glucosensing property in rat and human activated microglia. Neurobiol Dis 17:1-9.

Rodriguez MJ, Martínez-Sánchez M, Bernal F, Mahy N. 2004. Heterogeneity between hippocampal and septal astroglia as a contributing factor to differential in vivo AMPA excitotoxicity. J Neurosci Res 77(3):344-53.

Rodriguez MJ, Ursu G, Bernal F, Cusí V, Mahy N. 2001. Perinatal human hypoxia-ischemia vulnerability correlates with brain calcification. Neurobiol Dis 8:59-68.

Rolls A, Shechter R, London A, Segev Y, Jacob-Hirsch J, Amariglio N, Rechavi G, Schwartz M. 2008. Two faces of chondroitin sulfate proteoglycan in spinal cord repair: a role in microglia/macrophage activation. PLoS Med 5(8):e171.

Shaked I, Tchoresh D, Gersner R, Meiri G, Mordechai S, Xiao X, Hart RP, Schwartz M. 2005. Protective autoimmunity: interferon-gamma enables microglia to remove glutamate without evoking inflammatory mediators. J Neurochem 92(5):997-1009.

Simard JM, Chen M, Tarasov KV, Bhatta S, Ivanova S, Melnitchenko L, Tsymbalyuk N, West GA, Gerzanich V. 2006. Newly expressed SUR1-regulated $NC_{Ca\text{-}ATP}$ channel mediates cerebral edema after ischemic stroke. Nat Med 12(4):433-440.

Simard JM, Tsymbalyuk N, Tsymbalyuk O, Ivanova S, Yurovsky V, Gerzanich V. 2010. Glibenclamide Is Superior to Decompressive Craniectomy in a Rat Model of Malignant Stroke. Stroke 41(3):531-7.

Simard JM, Yurovsky V, Tsymbalyuk N, Melnichenko L, Ivanova S, Gerzanich V. 2009. Protective effect of delayed treatment with low-dose glibenclamide in three models of ischemic stroke. Stroke 40(2):604-9.

Stellwagen D, Malenka RC. 2006. Synaptic scaling mediated by glial TNF-α. Nature 440(7087):1054-9.

Streit WJ. 2002. Microglia as neuroprotective, immunocompetent cells of the CNS. Glia 40(2):133-9.

Streit WJ. 2005. Microglia and neuroprotection: implications for Alzheimer's disease. Brain Res Brain Res Rev 48(2):234-9.

Thored P, Heldmann U, Gomes-Leal W, Gisler R, Darsalia V, Taneera J, Nygren JM, Jacobsen S-EW, Ekdahl CT, Kokaia Z and others. 2009. Long-term accumulation of microglia with proneurogenic phenotype concomitant with persistent neurogenesis in adult subventricular zone after stroke. Glia 57(8):835-849.

Van Groen T, Puurunen K, Mäki H-M, Sivenius J, Jolkkonen J. 2005. Transformation of diffuse β-amyloid precursor protein and β-amyloid deposits to plaques in the thalamus after transient occlusion of the middle cerebral artery in rats. Stroke 36(7):1551-6.

Veroni C, Gabriele L, Canini I, Castiello L, Coccia E, Remoli ME, Columba-Cabezas S, Aricò E, Aloisi F, Agresti C. 2010. Activation of TNF receptor 2 in microglia promotes induction of anti-inflammatory pathways. Mol Cell Neurosci 45(3):234-44.

Wake H, Moorhouse AJ, Jinno S, Kohsaka S, Nabekura J. 2009. Resting microglia directly monitor the functional state of synapses in vivo and determine the fate of ischemic terminals. J Neurosci 29(13):3974-80.

Walberer M, Nedelmann M, Ritschel N, Mueller C, Tschernatsch M, Stolz E, Bachmann G, Blaes F, Gerriets T. 2010. Intravenous immunoglobulin reduces infarct volume but not edema formation in acute stroke. Neuroimmunomodulation 17(2):97-102.

Weston RM, Jones NM, Jarrott B, Callaway JK. 2007. Inflammatory cell infiltration after endothelin-1-induced cerebral ischemia: histochemical and myeloperoxidase correlation with temporal changes in brain injury. J Cereb Blood Flow Metab 27(1):100-14.

Wheeler A, Wang C, Yang K, Fang K, Davis K, Styer AM, Mirshahi U, Moreau C, Revilloud J, Vivaudou M and others. 2008. Coassembly of different

sulfonylurea receptor subtypes extends the phenotypic diversity of ATP-sensitive potassium (KATP) channels. Mol Pharmacol 74(5):1333-44.

Yamada K, Ji JJ, Yuan H, Miki T, Sato S, Horimoto N, Shimizu T, Seino S, Inagaki N. 2001. Protective Role of ATP-Sensitive Potassium Channels in Hypoxia-Induced Generalized Seizure. Science 292(5521):1543-1546.